Supporting information

Harnessing Laser Technology to Create Stable Metal Halide Perovskite-rGO Conjugates as Promising Electrodes for Zn-Ion Capacitors

Athanasia Kostopoulou,*[,a] Dimitra Vernardou,*[,b] Nikolaos Livakas,[a] Konstantinos Brintakis,[a] Stylianos Daskalakis,[b] and Emmanuel Stratakis*[,a,c]

[a.] *Institute of Electronic Structure and Laser, Foundation for Research and Technology - Hellas, Heraklion, 71110 Crete, Greece.*

E-mails: akosto@iesl.forth.gr, stratak@iesl.forth.gr

[b.] *Department of Electrical & Computer Engineering, School of Engineering, Hellenic Mediterranean University, Heraklion,710 04 Crete, Greece.*
Email: dvernardou@hmu.gr

[c.] *Department of Physics, University of Crete, 71003 Heraklion, Greece*

1. Characterization of the materials

i) ***Transmission Electron Microscopy (TEM).*** TEM images were captured on a LaB6 JEOL 2100 transmission electron microscope (JEOL Ltd, Akishima, Tokyo, Japan) operating at an accelerating voltage of 200 kV. All the images were recorded by the Gatan ORIUS TM SC 1000 CCD camera (Gatan Inc. Pleasanton, CA, USA). For the TEM observation, a drop of each dispersion was placed onto a carbon-coated copper TEM grid and let to evaporate.
ii) ***Scanning Electron Microscopy (SEM).*** SEM images were collected using a JSM-6390LV instrument with tungsten filament. The samples were dried onto silicon substrates before the experiments.
iii) ***X-ray diffraction (XRD).*** Grazing incident XRD pattern was recorded using a Bruker D8 Advance XRD equipment with Cu Kα1 radiation (λ = 1.5406 Å) and a power source of 40 kV and 40 mA. The measurements were performed at room temperature from 10 to 50 degrees with a step of 0.02 degrees and a rate of 5 seconds/step. The XRD patterns from the perovskite nanocrystals and conjugates were collected after drop-casting their colloidal dispersion onto glass substrates and let for drying.
iv) ***UV -Vis Spectroscopy.*** The UV-Vis absorption spectra of the colloidal nanocrystal dispersion were placed in quartz cuvettes and measured using a Perkin Elmer, Lamda 950 UV/VIS/NIR spectrophotometer.
v) ***Photoluminescence (PL) Spectroscopy.*** The PL emission of the dispersions were measured at room temperature utilizing a Fluoromax Phosphorimeter (Horiba Ltd., Kyoto, Japan) with a 150 W Xenon continuous output ozone-free lamp. The dispersion was placed in quartz cuvettes for the measurements.
vi) ***Raman Spectroscopy.*** Raman experiments were carried out using a Nicolet Almega XR Raman spectrometer (Thermo Fisher Scientific, Waltham, MA, USA) with 473 nm laser. The samples from the dispersions were dried onto silicon substrates before the experiments whereas the rGO powder was measured without dispersion.
vii) ***Atomic Force Microscopy (AFM).*** AFM experiments using tapping mode were employed in the Multimode Atomic Force Microscope from Digital Instruments, Bruker. The dispersions were deposited trough drop-casting onto silicon substrates and they dried before the measurements.

2. Metal halide perovskite nanocrystals synthesis and characterization

i) Materials

Cesium bromide (CsBr, 99.999%), lead (II) bromide ($PbBr_2$, trace metals basis, 98%), oleic acid (technical grade, $C_{18}H_{34}O_2$, 90%), oleylamine (technical grade, $C_{18}H_{37}N$, 70%), N,N-dimethylformamide (DMF, C_3H_7NO, reagent, >99.9%), toluene (C_7H_8, ACS reagent, ≥99.5%). All chemicals were received from Sigma-Aldrich and used without any treatment.

ii) Synthesis

$CsPbBr_3$ nanocrystals were synthesized by a precipitation-based protocol at ambient conditions reported by Li et al with slight modifications.[1] Specifically, 0.2 mmole $PbBr_2$ and 0.4 mmole CsBr were dissolved in 5 ml DMF and then 0.5 mL oleic acid (OA) and 0.25 mL oleylamine (Olam) were added in this stock solution. Following this procedure, 0.3 mL of the precursor stock solution was added dropwise in 5 ml of toluene under vigorous stirring (1200 rpm) and the solution let for stirring for 5 minutes. The color of the solution under a UV lamp is changing during the addition of the stock solution (Figure S1). The nanocrystals have been centrifuged two times to remove the excess

of reactants: i) 6000 rpm for 10 minutes, the precipitated product re-dispersed in toluene and ii) 700 rpm for 7 minutes, the supernatant was collected.

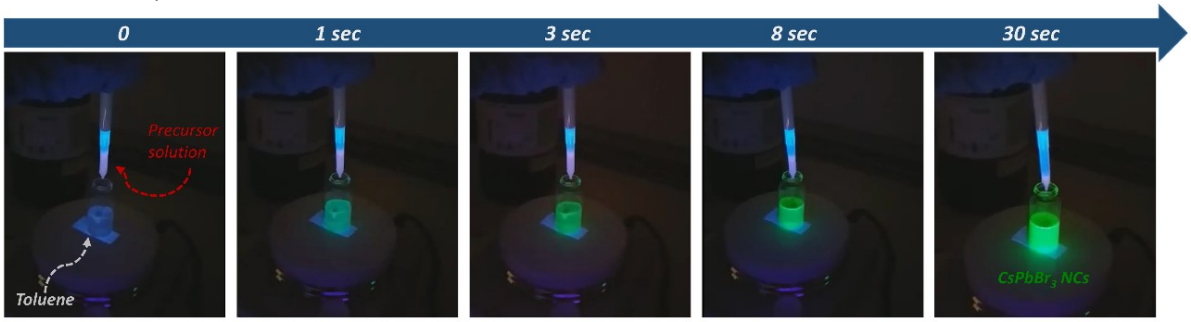

Figure S1. Digital photographs of the time evolution of metal halide perovskite nanocrystals formation after the addition of the precursor stock solution in the "bad" solvent (toluene) under a UV lamp.

iii) Morphological/structural features and optical properties of the metal halide perovskite nanocrystals

The as-prepared nanocubes were quite monodispersed in size, exhibiting a narrow size distribution with edge length of 10.9 ± 2.1 nm (Figure S2a). The crystallinity of the nanocrystals was confirmed by the grazing incident XRD pattern, and the Bragg reflection peaks can be indexed to the orthorhombic $CsPbBr_3$ crystal structure (COD 4510745) (Figure S2c).

The nanocrystal solution after the centrifugation and redispersion in toluene was photoluminescent active. A single and narrow PL peak (FWHM of 17.4 nm) centered at 501 nm was observed. The cyan-green emitting PL of nanocrystal solution can be attributed to weak quantum confinement effects due to nanocrystals with dimensions below Bohr radius (7 nm).[2, 3,4] The energy gap of the $CsPbBr_3$ nanocrystals calculated to be 2.45 eV from the Tauc plot (Figure S2b).

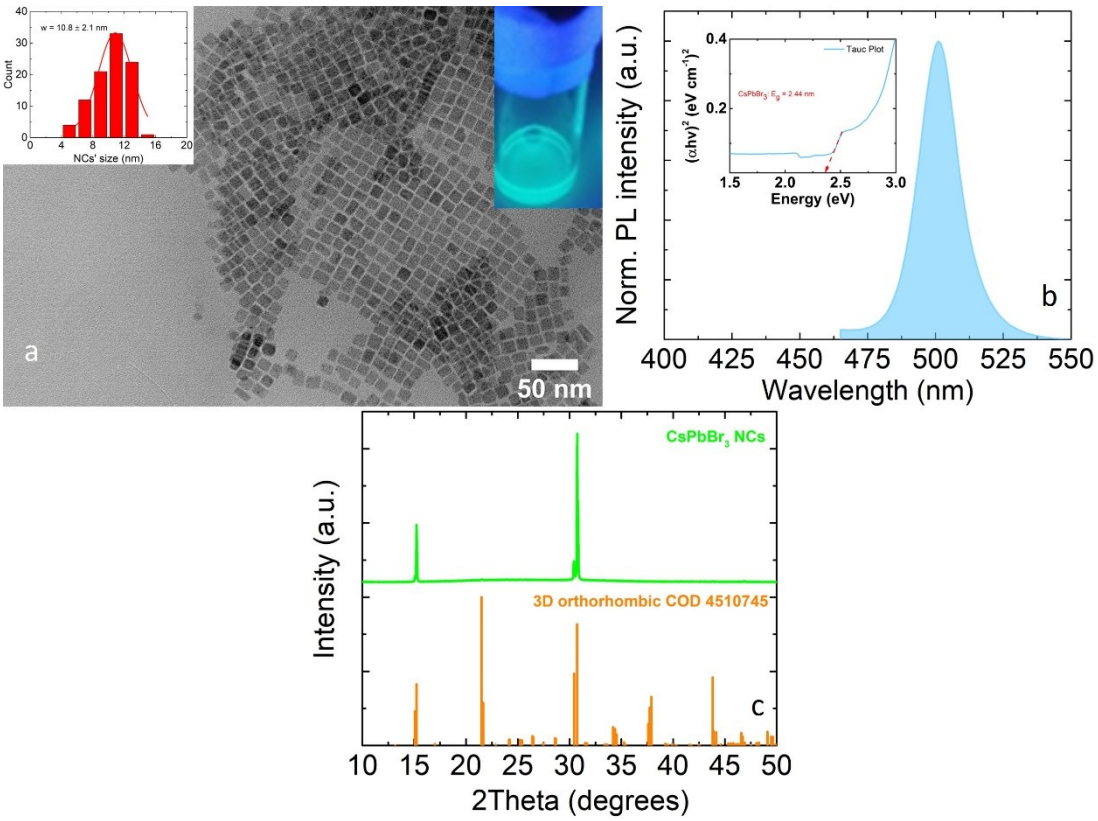

Figure S2. TEM image (a), PL spectrum (b) and grazing incident XRD pattern (c) of the metal halide perovskite nanocrystals fabricated for the conjugation with the rGO. Insets: Size distribution diagram and digital photo of nanocrystal dispersion under UV lamp (a), Tauc Plot of the UV-visible absorption data for the calculation of band gap energy (b).

3. Reduced graphene oxide dispersion in toluene

i) Materials

Amine functionalized reduced graphene oxide (rGO-NH_2, powder, Carbon, >65 wt. %, Nitrogen, >5 wt. %), toluene (C_7H_8, hydrous reagent), All chemicals were received from Sigma-Aldrich.

ii) rGO sheets dispersion

Liquid phase exfoliation of the commercial rGO powder was employed in order to obtain rGO thinner sheets dispersed in toluene (the common solvent with the perovskite nanocrystals). Specifically, 5 mg of the amine-functionalized reduced graphene oxide was dispersed in 6 ml toluene and placed in the sonication bath for 1 hour.

iii) Morphological features of the rGO sheets

The exfoliation and the reduction of the sheets' size of the commercial amine-functionalized rGO were confirmed from the combination of the results from the SEM, TEM and AFM (Figure S3). Sheets with lateral sizes in the order of several microns were revealed from SEM and TEM images for the exfoliated sample while an average thickness of 2.3 ± 0.2 nm was determined from AFM. Before the exfoliation, the thickness of the rGO flakes was 7.5 ± 0.5 nm. The reduced thickness was also revealed with TEM from the different contrast between the sheets before and after the exfoliation process.

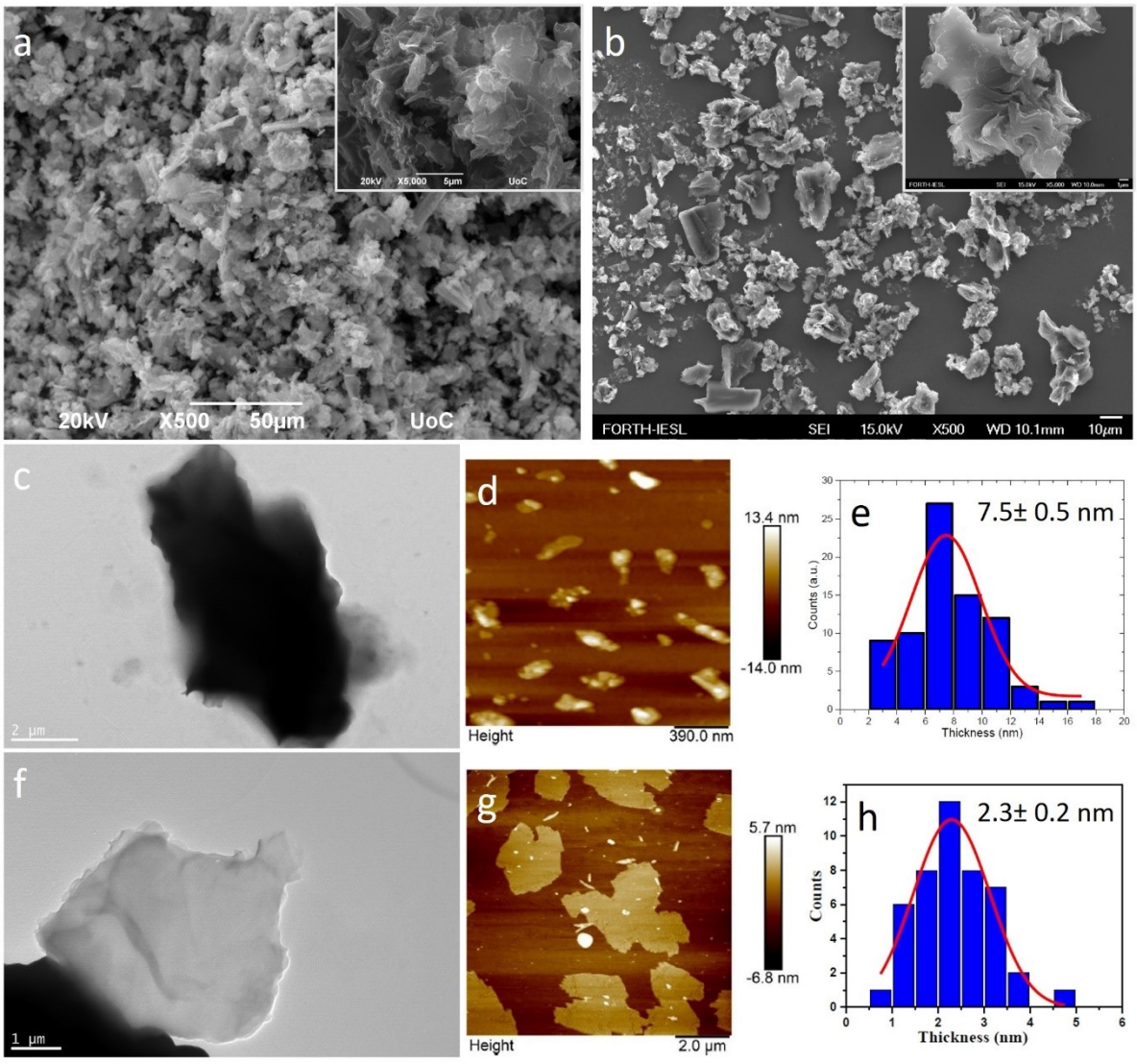

Figure S3. SEM (a, b), TEM (c, f) and AFM (d, g) images of the NH_2-functionalized rGO sheets before and after liquid-phase exfoliation. Thickness distribution diagrams of the thickness calculated from the AFM images (e, h).

4. Photo-induced conjugation of perovskite nanocrystals on rGO sheets: Set up and irradiation conditions

The setup used for conjugation of the two materials was described in our previous publications. [5,6] It was consisted of an Yb:KGW ultrafast pulsed laser source, two mirrors and a convex lens of 20 cm focal length (Figure S4). Contrary to our previous reports, a different laser was used for these experiments and continuous stirring was applied in order to obtain homogenous distribution of the perovskite nanocrystals on the rGO sheets. A laser of 1026 nm laser was utilized in order not to affect the small perovskite nanocrystals by the irradiation. The laser source emitted linearly polarized pulses with 170 femtoseconds at 60 kHz repetition rate at 1026 nm wavelength. The nanocrystals and the NH_2 functionalized rGO in the common solvent were placed in a vial and fixed 5 cm out of focus length. The Gaussian spot diameter was 700 μm at $1/e^2$, which measured and analyzed utilizing a CCD camera. The laser fluence fixed for all the irradiation experiments at 0.5 mJ/cm^2.

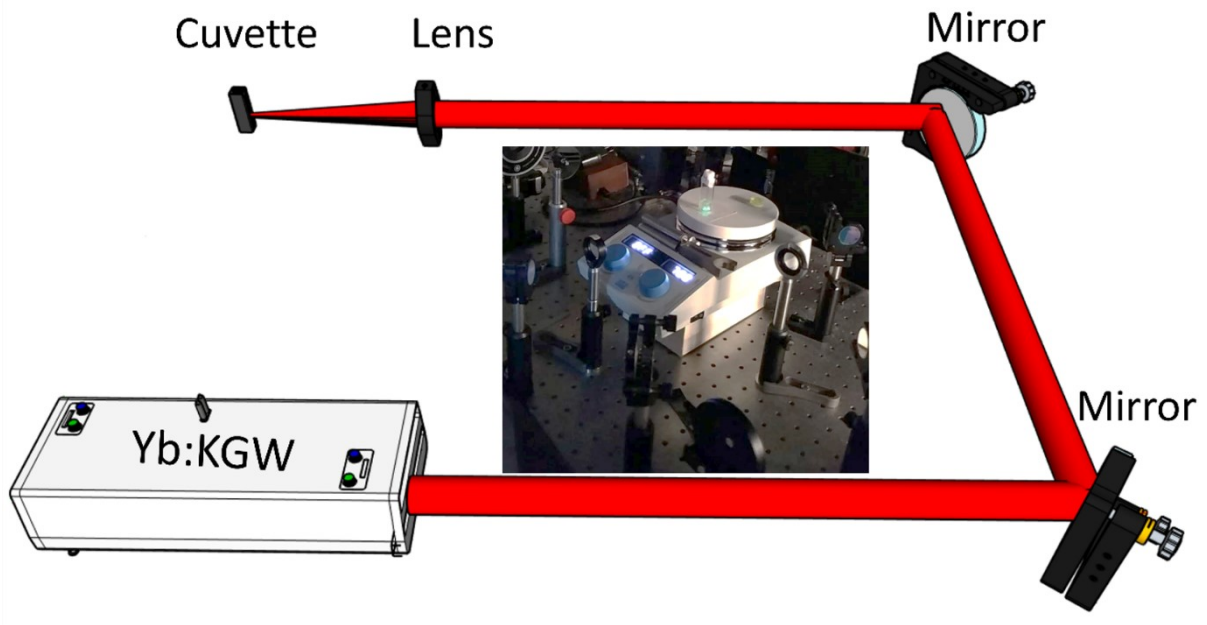

Figure S4. Schematic representation of the setup used for the conjugation of the metal halide perovskites with the rGO sheets utilizing a femtosecond pulsed laser of 1026 nm wavelength.

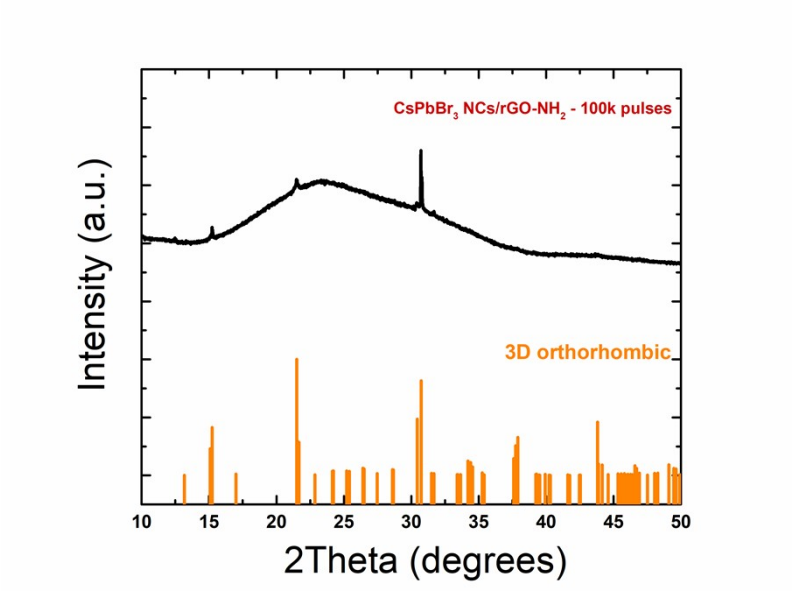

Figure S5. Grazing incident XRD pattern of the metal halide perovskite-rGO conjugates after irradiation with 10^5 number of pulses.

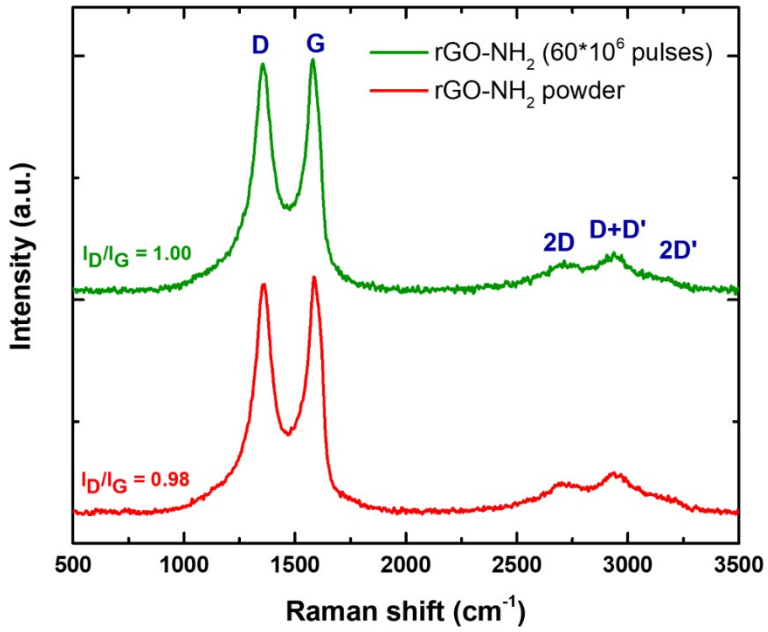

Figure S6. Raman spectra of the NH_2-functionalized rGO, before (red curve) and after laser irradiation upon 60 million pulses (green curve).

5. Electrodes fabrication and electrochemical characterization

The metal halide perovskite nanocrystal-rGO conjugates, pure rGO and perovskite nanocrystal were deposited on Ni foil, with thickness 0.5 mm (99.98% trace metals basis), which was purchased from Sigma Aldrich. The deposition was accomplished by drop casting using toluene-based solution and then adding a thin layer of TiO_x through Pulsed Laser Deposition (PLD). TiO_2 targets used in PLD for the coverage were prepared by pressing 1 g of 99 % pure TiO_2 powder purchased from Sigma Aldrich at room temperature under 4 tons for 2 min. Pulsed laser ablation of the solid targets and subsequent sample coverage were performed into a high vacuum (3x 10^{-6} mbar) chamber, using a KrF laser (excimer laser with 248 nm wavelength, 20 ns pulse duration and 10 Hz pulse repetition rate) emitting an energy density (fluence) of 2 J·cm^{-2}. Adjusting the focusing lens, the laser spot size was optimized and an optical attenuator was used to tune the laser fluence. The target-to-substrate distance was adjusted to 5 cm and the optimum laser pulses number to 1000.

The electrochemical performance of the anode materials was evaluated in a three-electrode electrochemical cell utilizing the anode materials, Pt and Ag/AgCl as working, counter and reference electrodes, respectively. An aqueous solution of 0.5 M $ZnSO_4$ acted as an electrolyte during all measurements for a potential window of -0.5 V to +1.0 V and a scan rate of 100 mV·s^{-1}. In order to understand the mechanisms taking place during the Zn^{2+} intercalation/deintercalation processes, scan rates ranging from 4 mV·s^{-1} to 10 mV·s^{-1} were studied. The galvanostatic measurements were also performed at an applied specific current of 0.8 A g^{-1} in the potential range between -0.5 V to +1.0 V vs. Ag/AgCl.

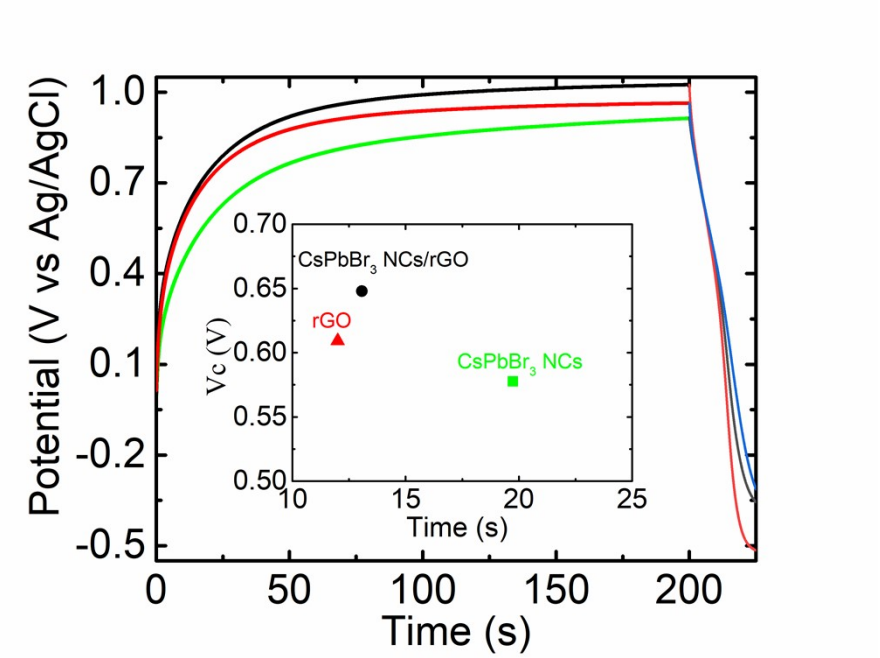

Figure S7. Time dependence of the potential for the conjugations (black), pure rGO (red) and pure perovskite nanocrystals (green) electrodes.

Table S1. All-inorganic hybrid graphene-based composites for capacitors. The capacitance enhancement of the hybrid/conjugated systems compared to the capacitance of the rGO used in each work has been calculated from the equation: Enhancement (%)= $[(C_{hybrid}-C_{rGO})/C_{rGO}]*100$, where C_{hybrid} and C_{rGO} the capacitances of the hybrid material and rGO respectively.

Hybrid composites	$C_{composite}$ (F/g)	$C_{2D\ material}$ (F/g)	Conditions	Enhancement (%)	Ref
Zn/rGO	33.88	20.78	At 10 mV s^{-1} in 1 M H_2SO_4	63	[7]
MnO_2/rGO	135.5	74.5	At 40 mV s^{-1} in1 M Na_2SO_4	81.8	[8]
Co_3O_4/rGO	291	56	At 1 A g^{-1} in 6 M KOH	419.6	[9]
Fe_3O_4/rGO	480	139	At 5 A g^{-1} in 1 M KOH	245.3	[10]
ZnO/rGO	308	157	At 1 A g^{-1} in 0.1 M Na_2SO_4	96.2	[11]
ZnO/Gr	11.3	~1.5	At 10 mVs^{-1} in 1 M KCl	653.3	[12]
SnO_2/Gr	34.6	20.7	At 1.0 V s^{-1}, 1 M H_2SO_4	67.1	[13]
Co_3O_4/Gr	243	169.3	At 10 mV s^{-1} in 6 M KOH	43.53	[14]
$Co(OH)_2$/Gr	972.5	137.6	At 5 mV s^{-1} in 6 M KOH	606.8	[15]
CeO_2/Gr	191	81.57	At 5 mV s^{-1} in 3 M KOH	134.2	[16]
MnO_2/Gr	320	34	At 10 mV s^{-1} in 1 M of Na_2SO_4	841.2	[17]
Fe_3O_4/Gr	169	101	At 1 Ag^{-1} in 1 M KOH	67.3	[18]
MnO_2/Gr	310	104	At 2 mV s^{-1} in 1 M Na_2SO_4	198	[19]
Carbon Black/Gr	138	11.2	At 10 mV s^{-1} in 6 M KOH	1132	[20]
Pt/Gr	269	14	In 0.5 N H_2SO_4	1821	[21]
MnO_2/Gr	389	93	At 1 A g^{-1} in 1 M Na_2SO_4	318.3	[22]
$MnSiO_3$/GO	262.5	4.6	At 0.5 A g^{-1} in 1 M Na_2SO_4	5606	[23]
MnO_2/GO	197.2	10.9	At 200 mA g^{-1} in 1 M Na_2SO_4	1709	[24]
Silver-doped MnO_2/GO	877	195	At 5 mV s^{-1}in 1 M of Na_2SO_4	349.7	[25]
MnO_2/G	124	<2	At 2 mV s^{-1} in 1 M Na_2SO_4	6100	[26]
MnO_2/G	158	<2	At 2mAcm^{-2} in 2 M $(NH_4)_2SO_4$	7800	[27]
Zn-ion capacitors					
NbPO/rGO	191.88		At 1 A g^{-1} in 0.2 M $ZnSO_4$		[28]
Carbon nanotubes/rGO	41.7		At 1 mV s^{-1} in 2 M (PVA)/$Zn(CF_3SO_3)_2$		[29]
$Co_xNi_{2-x}P$/rGO	356.6		At 0.5 A g^{-1} in 2 M $ZnSO_4$		[30]
Our work	**107**	**0.600**	At 0.8 A g^{-1} in 0.5 M $ZnSO_4$	**17733**	

References

1 X. Li, Y. Wu, S. Zhang, B. Cai, Y. Gu, J. Song and H. Zeng, *Advanced Functional Materials*, 2016, **26**, 2435–2445.
2 L. Protesescu, S. Yakunin, M. I. Bodnarchuk, F. Krieg, R. Caputo, C. H. Hendon, R. X. Yang, A. Walsh and M. V. Kovalenko, *Nano Lett.*, 2015, **15**, 3692–3696.
3 Q. A. Akkerman, S. G. Motti, A. R. Srimath Kandada, E. Mosconi, V. D'Innocenzo, G. Bertoni, S. Marras, B. A. Kamino, L. Miranda, F. De Angelis, A. Petrozza, M. Prato and L. Manna, *Journal of the American Chemical Society*, 2016, **138**, 1010–1016.
4 L. Protesescu, S. Yakunin, M. I. Bodnarchuk, F. Krieg, R. Caputo, C. H. Hendon, R. X. Yang, A. Walsh and M. V. Kovalenko, *Nano letters*, 2015, **15**, 3692–6.
5 A. Kostopoulou, K. Brintakis, E. Serpetzoglou and E. Stratakis, *Nanomaterials*, 2020, **10**, 747.
6 A. Kostopoulou, K. Brintakis, M. Sygletou, K. Savva, N. Livakas, M. A. Pantelaiou, Z. Dang, A. Lappas, L. Manna and E. Stratakis, *Nanomaterials*, 2022, **12**, 703.
7 M. Ates, S. Caliskan and E. Özten, *J Solid State Electrochem*, 2018, **22**, 3261–3271.
8 Z. Li, J. Wang, S. Liu, X. Liu and S. Yang, *Journal of Power Sources*, 2011, **196**, 8160–8165.
9 H.-W. Wang, Z.-A. Hu, Y.-Q. Chang, Y.-L. Chen, Z.-Y. Zhang, Y.-Y. Yang and H.-Y. Wu, *Materials Chemistry and Physics*, 2011, **130**, 672–679.
10 W. Shi, J. Zhu, D. H. Sim, Y. Y. Tay, Z. Lu, X. Zhang, Y. Sharma, M. Srinivasan, H. Zhang, H. H. Hng and Q. Yan, *J. Mater. Chem.*, 2011, **21**, 3422–3427.
11 Y.-L. Chen, Z.-A. Hu, Y.-Q. Chang, H.-W. Wang, Z.-Y. Zhang, Y.-Y. Yang and H.-Y. Wu, *J. Phys. Chem. C*, 2011, **115**, 2563–2571.
12 Y. Zhang, H. Li, L. Pan, T. Lu and Z. Sun, *Journal of Electroanalytical Chemistry*, 2009, **634**, 68–71.
13 F. Li, J. Song, H. Yang, S. Gan, Q. Zhang, D. Han, A. Ivaska and L. Niu, *Nanotechnology*, 2009, **20**, 455602.
14 J. Yan, T. Wei, W. Qiao, B. Shao, Q. Zhao, L. Zhang and Z. Fan, *Electrochimica Acta*, 2010, **55**, 6973–6978.

15 S. Chen, J. Zhu and X. Wang, *J. Phys. Chem. C*, 2010, **114**, 11829–11834.
16 Y. Wang, C. X. Guo, J. Liu, T. Chen, H. Yang and C. M. Li, *Dalton Trans.*, 2011, **40**, 6388–6391.
17 M. N. Dang, T. H. Nguyen, T. V. Nguyen, T. V. Thu, H. Le, M. Akabori, N. Ito, H. Y. Nguyen, T. L. Le, T. H. Nguyen, V. T. Nguyen and N. H. Phan, *Nanotechnology*, 2020, **31**, 345401.
18 Q. Ke, C. Tang, Y. Liu, H. Liu and J. Wang, *Mater. Res. Express*, 2014, **1**, 025015.
19 J. Yan, Z. Fan, T. Wei, W. Qian, M. Zhang and F. Wei, *Carbon*, 2010, **48**, 3825–3833.
20 G. Wang, X. Sun, F. Lu, H. Sun, M. Yu, W. Jiang, C. Liu and J. Lian, *Small*, 2012, **8**, 452–459.
21 Y. Si and E. T. Samulski, *Chem. Mater.*, 2008, **20**, 6792–6797.
22 B. G. Choi, M. Yang, W. H. Hong, J. W. Choi and Y. S. Huh, 3D Macroporous Graphene Frameworks for Supercapacitors with High Energy and Power Densities, https://pubs.acs.org/doi/pdf/10.1021/nn3003345, (accessed February 15, 2023).
23 Y. Cheng, Y. Zhang, Q. Wang and C. Meng, *Colloids and Surfaces A: Physicochemical and Engineering Aspects*, 2019, **562**, 93–100.
24 S. Chen, J. Zhu, X. Wu, Q. Han and X. Wang, *ACS Nano*, 2010, **4**, 2822–2830.
25 V. J. Mane, S. B. Kale, S. B. Ubale, V. C. Lokhande and C. D. Lokhande, *Materials Today Chemistry*, 2021, **20**, 100473.
26 C. Wan, K. Azumi and H. Konno, *Electrochimica Acta*, 2007, **52**, 3061–3066.
27 J. Yan, Z. Fan, T. Wei, Z. Qie, S. Wang and M. Zhang, *Materials Science and Engineering: B*, 2008, **151**, 174–178.
28 S. J. Patil, N. R. Chodankar, S.-K. Hwang, G. S. R. Raju, K. S. Ranjith, Y. S. Huh and Y.-K. Han, *Energy Storage Materials*, 2022, **45**, 1040–1051.
29 T. Ni, S. Wang, J. Shi, X. Du, Q. Cheng, Z. Dong, L. Ruan, W. Zeng, X. Guo, X. Ren and Z. Huang, *Advanced Materials Technologies*, 2020, **5**, 2000268.
30 D. Guo, Z. Li, D. Wang, M. Sun and H. Wang, *ChemSusChem*, 2021, **14**, 2205–2215.